Recycling of Zircaloy Machining Chips Using Powder Metallurgy and Remelting in an Electric Arc Furnace

Article *in* Advances in Materials Science and Engineering · December 2017

CITATIONS
0

READS
40

4 authors, including:

Luis Gallego Martinez
University of São Paulo
99 PUBLICATIONS **284** CITATIONS

SEE PROFILE

Research Article

Advances in Materials Science and Engineering

Recycling of Zircaloy Machining Chips Using Powder Metallurgy and Remelting in an Electric Arc Furnace

Pereira LAT*, Martinez LG, Rossi JL and Takiishi H

Materials Science and Technology Center - CCTM, Nuclear and Energy Research Institute, IPEN - CNEN/SP, Av. Prof. Lineu Prestes, 2242, São Paulo 05508-000, SP, Brazil

***Corresponding author**
Pereira LAT, Materials Science and Technology Center - CCTM, Nuclear and Energy Research Institute, IPEN - CNEN/SP, Av. Prof. Lineu Prestes, 2242, São Paulo 05508-000, SP, Brazil, Email: luiz.atp@uol.com.br

Submitted: 14 Nov 2017; **Accepted**: 30 Nov 2017; **Published**: 22 Dec 2017

Abstract

Nuclear power reactors use UO_2 pellets as nuclear fuel and Zircaloy as cladding. Machining chips are generated in the fabrication of Zircaloy. This highly valuable material is not discarded for regular recycling due to its low market price. This paper presents two methods for recycling Zircaloy chips. The first is the powder metallurgy technique, where by the chips were subjected to hydriding, which involved milling, isostatically pressing and sintering the material. The second technique consisted of melting the chips in an electric arc furnace to obtain ingots, which were heat-treated. The chemical composition, crystal phases, hardness and microstructures produced by the two methods were characterized, strongly suggesting that Zircaloy chips maybe a source of high quality material that can be reused in the field of nuclear technology and in biomaterials.

Keywords: Powder metallurgy, Zircaloy, Recycling, Nuclear fuel, Cladding, Hydriding, Electric arc melting

Introduction

UO_2 pellets used as nuclear fuel for power reactors are usually coated with zirconium alloy cladding tubes, which, together with the structural components of the fuel elements, are exposed to aqueous environments under high-pressure, temperature, and high neutron flux [1]. Thus, cladding should have excellent mechanical and corrosion properties and a low thermal neutron absorption cross section. Hafnium-free zirconium alloys have these properties because of their good neutron absorption, chemical composition, and microstructure. Each tube is closed at its ends by a plug that is also made of Zr alloy and is machined from massive metal bars. During the manufacture of this component, large amounts of chips are generated by machining in automatic lathes. Nuclear-grade zirconium alloys are considered strategic materials that are very expensive and not freely commercialized. As part of a strategy to produce nuclear fuels in Zr alloys using an autonomous infrastructure, the Zircaloy machining chips resulting from the nuclear power generation process represent a valuable source of spent fuel elements and zirconium evaluated in these conditions is worth US$ 40 to 80/kg [2]. This is because Zr metal, which is the major constituent of Zircaloy-4alloy (alloy Zry-4), has the significant advantage of being Hf-free [3]. The other most common alloys are called Zircaloy-2, ZIRLO® and M5®, whose elemental compositions are described in Table 1. Another commonly used zirconium alloy is PCA-2b, which is not well documented in the open literature.

This study focused on improving the recycling of Zircaloy machining chips, using the powder metallurgy technique and remelting in an electric arc furnace. A methodology was specially developed using powder metallurgy techniques, based on the metal embrittlement effect caused by the action of hydrogen to demonstrate the feasibility of producing cladding end caps using the near net shape approach [4,5].

Table 1: Typical nominal (mass %) compositions of Zircaloy-2, Zircaloy-4, ZIRLO® and M5® alloy

Alloy / Element	Sn	Fe	Cr	Ni	O	Hf	Nb	Zr
Zircaloy-2	1.2-1.7	0.07-0.20	0.05-0.15	0.03–0.08	0.12	<1000 ppm	-	balance
Zircaloy-4	1.2-1.7	0.18-0.24	0.07-0.13	-	0.12	<1000 ppm	-	balance
ZIRLO®	0-0.99	0.11	-	-	0.11	40 ppm	0.98	balance
M5®	<30 ppm	0.03	40 ppm	-	0.14-0.15	-	1.00	balance

The aims of this work were therefore threefold: i) develop a new research line involving methods to recycle Zircaloy machining chips; ii) reduce the enormous volume of material stored in the form of machining chips by 30-fold by melting it, enabling it to be used in the manufacture of other components for the nuclear or biomaterials industry; and iii) conduct basic development research.

Materials and Methods

The Zircaloy-4 (Zry-4) raw material used in this study was supplied in the form of machining chips contaminated mainly with cutting oil. The conditioning treatment consisted initially of cleaning the material by means of manual magnetic separation to remove ferrous contamination before degreasing with detergent, rinsing in water, then acid pickling with HCl and HNO_3 aqueous solutions [8].

For the powder metallurgy study, pressed chips were placed in a stainless steel retort to hydride the alloy. The open side of the tube was connected to two pipes, one for the H_2 admixture and the other for vacuum pumping. The controlled heating ramp was set at 500°C [9]. After the temperature stabilized, H_2 was injected under 3 bar for Zry-4 hydriding. To obtain zirconium hydride powder, the zirconium hydride was ground in a ball mill containing cyclohexane and 5mm diameter ZrO_2 balls. The hydrided chips were ground in a planetary high energy mill. Milling was performed for 30, 45, and 60 minutes, and the resulting samples were identified as #1, #2 and #3, respectively. The particle size distribution was measured using a laser diffraction technique. The resulting powder was then encapsulated in a silicone mold and isostatically cold compacted under 200 MPa pressure. In the near net shape approach taken in this study, the shape of the silicone mold was similar to that of the cladding end caps. Figure 1 shows the raw materials, chips compressed into briquettes, Zr hydride powder, and the powder cold isostatic pressed into near final shape. The specific density of the sintered samples was measured by He_2 pycnometry, which measures the material's real volume.

The compacted hydride powder samples were put into a stainless steel retort, which was then inserted into a tubular resistance furnace. The operation was initiated by emptying the tube through a vacuum system connected to the tube, until the pressure reached 7×10^{-5} mbar. The furnace heating system was then turned on, applying a heating rate of 8 °C/min up to the desired temperature. As the temperature increased, the H_2 increased, thus decreasing the vacuum. After 2 h, the vacuum was recovered and stabilized at 4.8×10^{-6} mbar, indicating that the H_2 evolution rate and the vacuum pumping had reached equilibrium. At this point, samples #1, #2 and #3 were sintered for 20 h at 1070 ºC, for 10 h at 1150 ºC and for 10 h at 1150 ºC, respectively.

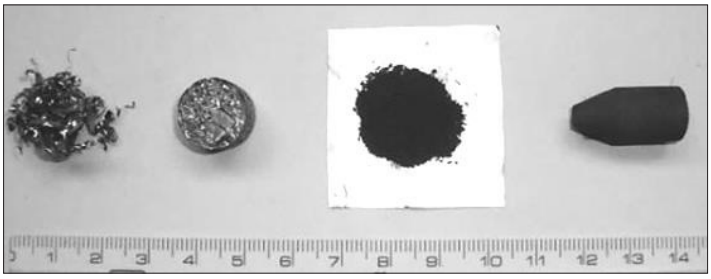

Figure 1: From left to right: as received machining chips, briquettes, Zr hydride powder and compressed sample

The chips were melted in a VAR (vacuum arc remelting) furnace fitted with a non-consumable tungsten electrode (W-2% ThO_2) under an inert gas atmosphere (Argon 99.998% purity); the VAR operated with 110 A current. The machining chips were pressed into small briquettes and bars measuring approximately $50 \times 10 \times 10$ mm^3. A total of 10 furnace loads were melted.

As for the machining chips remelted in the arc furnace, three of the 10 resulting melted ingots are discussed in the present study (samples #1, #2 and #3). Samples #1 and #2 were subjected to a thermomechanical treatment that consisted of annealing at 850 ºC and 950 ºC, respectively, followed by hot rolling in a two-high-four-high mill [10]. Sample #3 was cold-rolled (20% area reduction) after annealing at 910ºC. To prevent oxidation of the Zr alloy during furnace heating, all these samples were encapsulated in copper tubes. This procedure is explained in detail elsewhere [8,11].

The chemical composition of the samples was determined by energy dispersive X-ray fluorescence (EDXRF) spectroscopy. EDX elements were determined by the fundamental parameters method and a sensitivity curve was drawn using standards and certified materials [7,12]. The samples were cut with a diamond precision disk, embedded in cold-cure polyester resin, and sandpapered with 400 to 4000 grit SiC abrasive paper, followed by polishing with 6 µm and 1 µm diamond paste and final polishing with 0.06 µm colloidal silica. Etching was carried out using a solution of H_2O_2 50% + 25% HNO_3 + 25% ethanol + 2 drops HF and metallographic analysis was performed using optical (OM) and scanning electron microscopy (SEM) [13-15].

X-ray diffraction measurements were taken using a diffractometer equipped with a goniometer of 285 mm radius with theta-theta geometry, a pyrolytic graphite monochromator and a scintillation detector, using CuKα radiation, 40 kV voltage and 30 mA current. The melted samples analyzed by XRD were prepared by grinding the surfaces up to1200 grit.

Hardness was measured using the Rockwell hardness scale B (HR_B). For melted samples #1 and #2, hardness was measured along the transverse and longitudinal sections after hot rolling. This was done to verify the occurrence of hardness anisotropy due to mechanical working.

Results and Discussion

Table 2 compares the chemical specification for standard Zry-4 and the composition of the machining chips. As can be seen, the chemical composition and measured values of CRM 098 are in agreement with the certified values, thus validating the methodological analysis [16]. This analysis also indicates that the composition of the chips meets the specifications listed in Table 1. Table 2 describes the chemical compositions of samples obtained after melting the Zry-4 machining chips (sintered samples showed similar results). The chemical analysis of the samples listed in Table 2 indicates that almost all of contents of the alloy elements are equal to those of the specifications. However, Fe exceeds the specified content, indicating that contamination of the machining chips occurred and that this was not remediated during the cleaning treatment, except in sintered samples, which contained smaller Fe contents.

Table 2: Chemical analysis of Zry-4 chips, CRM 098 standard, Zr alloy obtained after melting Zry-4 machining chips and sintering, together with specification values for Zry-4 alloy using X-ray fluorescence spectroscopy

Element (mass %)	CRM 098 Certified values	CRM 098 measured values	Zry-4 chips measured values	Melted sample	Sintered sample	Zry-4 Specif
Cr	0.0906±0.009	0.088±0.003	0.080±0.010	0.066±0.003	0.070±0.002	0.07-0.13
Fe	0.2143± 0.002	0.210 ± 0.006	0.213 ±0.036	0.340± 0.030	0.293±0.012	0.18-0.24
Sn	1.460 ± 0.009	1.42 ±0.15	1.246 ±0.102	1.110± 0.030	1.295±0.043	1.2-1.7
Zr	balance	98.30±0.15	98.43+0.06	98.45±0.010	98.34+0.010	balance

Figure 2 shows the sintered samples as near net shape caps. Figure 3(a) illustrates the size and appearance of the melted Zry-4 ingots, and the same samples after hot rolling and after removal of the encapsulation. The hot-rolled ingots showed a reduction of section area of 27% and 32% in samples #1 and #2, respectively, as can be observed in Figure 3(b).

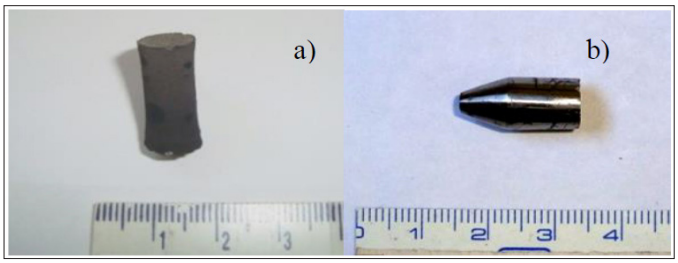

Figure 2: Sintered samples: (a) sample #2 and (b) sample #3 sintered as a cap with almost final geometry. Author: Pereira, LAT

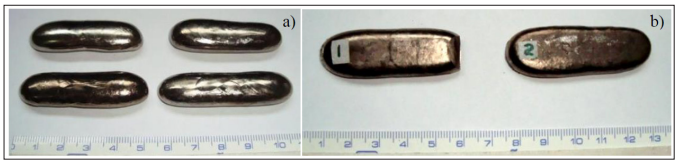

Figure 3: a) Ingots obtained in VAR furnace after melting Zry-4 machining chips. b) Samples #1 and #2 after hot-rolling and removal of encapsulation. Author: Pereira, LAT

The SEM micrograph in Figure 4 illustrates the morphology of the hydride powder particles after milling, while Figure 5 shows the microstructure of sintered sample #3. In Figure 5, note that the microstructure consists of equiaxed grains with α phase and with some lamellae in the grains. Although residual hydrogen is a beta-stabilizer, this phase was not detected by X-ray diffraction. The other structures in the microstructure are currently under study.

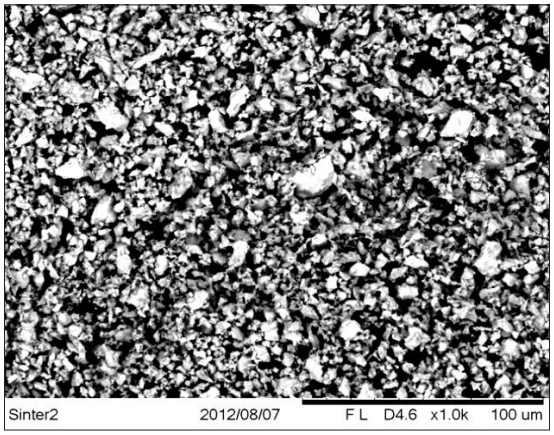

Figure 4: SEM micrograph of ZrH_2 powder used in sintering sample #2, showing angular particle morphology

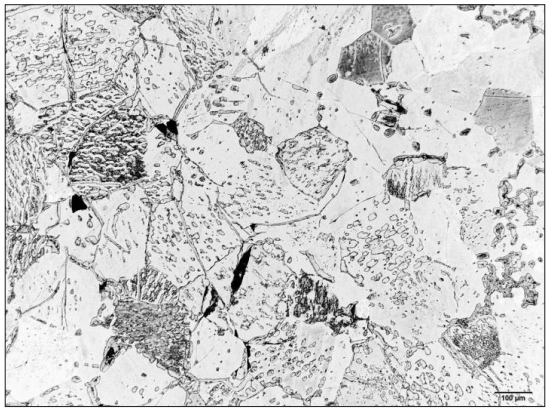

Figure 5: SEM microscopy recorded after sintering sample #3

Table 3 lists the average size of hydride Zircaloy-4 powder particles as a function of different milling times.

Specific densities of sintered samples #1, #2 and #3 were measured using He2 pycnometry and are listed in Table 4, together with the fraction of the theoretical density for Zircaloy.

It was found that reducing the particle size of hydride powder increased the real density of the sintered samples. This was attributed to the increased interparticle contact area in the green samples.

Table 3: Particle size of zirconium hydride powder measured as a function of different milling times

Milling time (mm)	30	45	60
Average diameter (μm)	5.06	3.17	2.09
Diameter-d50% (μm)	5.23	2.37	1.64

Table 4: Measured densities of sintered samples #1, #2 and #3

Sintered samples	Sample #1	Sample #2	Sample #3
Specific density (g/cm^3)	5.01	6.18	6.44
Fraction of the theoretical specific density (%)	77	95	95 98

However, despite the larger interparticle contact area, the green density was apparently unaffected and the driving force for solid-state sintering was improved, since the sintering rate depends on the particle radius. Thus, powder with a finer particle size distribution allows for better sintering (faster and at lower temperatures) than coarser particles. In addition, the uniformity, shape and particle size distribution of the powder, which can also contribute to the final properties, was adequate, as indicated in Figure 4 [17].

Figure 6 shows the typical microstructure of the samples before heat treatment, while the optical micrograph in Figure 7 shows a

sample heated using the aforementioned temperature and rolling mill scheme. The fibers exhibit a parallel-type arrangement before rolling (lengths between 80 µm and 100 µm). After rolling, however, the fibers have a Widmanstätten basket weave configuration with smaller and finer fibers (lengths between 40 µm and 60 µm and thicknesses of approximately 5 µm) [18]. The optical micrograph of the rolled sample heated at 950 ºC (in Figure 7) reveals a morphology similar to the previous Widmanstätten basket weave type, with thickening of the fibers (thicknesses of 5 µm to 10 µm and lengths of 30 µm to 40 µm). Table 5 lists the Rockwell B hardness values measured from melted samples #1, #2 and #3 after thermomechanical treatment.

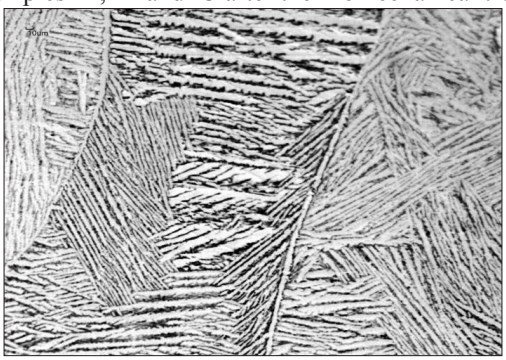

Figure 6: Optical micrograph of melted sample #1 before heat treatment, showing α phase in parallel slats

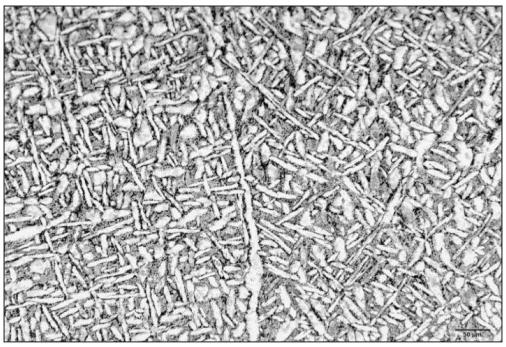

Figure 7: Optical micrograph of sample #2 after annealing at 950°C and hot rolling in α phase parallel slat layout

Table 5: HR_B hardness of samples measured before and after hot rolling (in the transversal and longitudinal directions). Authors: Pereira LAT, Martinez LG, Rossi JL, Takiishi H

Sample	1	2	3
Before rolling (HR_B)	-	-	93.0±0.5
Transversal secction (HR_B)	103.3±0.4	89±5	96±2
Longitudinal section (HR_B)	105.7±0.5	92.8±0.7	98.2±0.2

An explanation for the above values can be found in a binary diagram of Zr-Sn. Note that samples #1 and #2 were measured at the time of rolling in the α and β phases, respectively. According to deformation theory, the α phase is more difficult to deform, resulting in greater hardness, while sample #2 was more ductile because it was in the β phase, with lower hardness [19].

Figure 8 shows an X-ray diffraction pattern of the melted sample #4 plotted with the adjusted data, using the powder cell program. In addition to identifying the phases, the adjustment also provides the indices of diffracted planes and the lattice parameters. For comparison, Figure 9 depicts the XRD pattern of the samples shown in Figure 3 and plotted on the same graph.

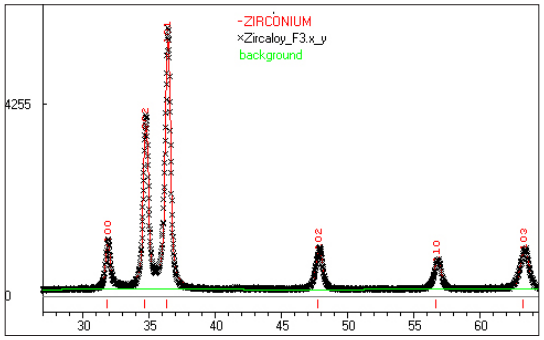

Figure 8: Refined XRD data of the Zircaloy-4 sample obtained by arc melting. The adjusted network parameters and indices shown in this figure indicate the phase was Zr

As can be seen in Figure 9, the XRD pattern revealed only the presence of Zr because of the low content of other chemical elements in the alloy and because the Zircaloy structure was kept in the form of solid solution. In this figure, note that the different rolling conditions did not interfere in the crystal structure of the samples. A comparison of each lattice parameter shown in Figure 8 (a = 3.2443 Å, c = 5.1669 Å) against the values of zirconium HC structure found in the literature (a = 3.232 Å, c = 5.147 Å) indicates that the Zircaloy samples had higher lattice parameters than those of pure Zr [19,20]. The differences between the lattice parameters of Zircaloy samples were attributed to the different amounts of gas (oxygen, hydrogen and nitrogen), alloying elements and microstructural conditions dissolved in the form of interstitial solution. This can cause distortion of the lattice and affect the planar distance (*d*), thus altering the peak width, given the codependency between 2θ and *d* at the same wavelength, according to Bragg's law shown below:

$$n\lambda = 2d\sin\theta.$$

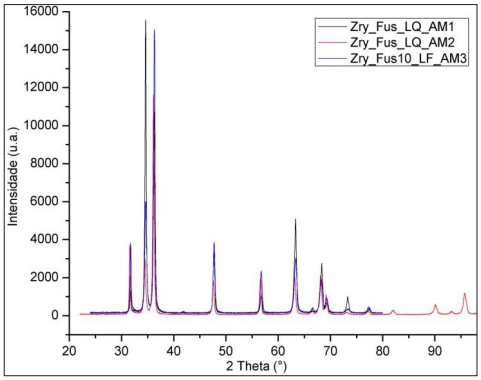

Figure 9: Superposed XRD pattern of rolled Zircaloy-4 samples

Conclusion

Based on the chemical analysis of the melted samples, it can be concluded that the original alloy composition of Zircaloy remained unchanged after it was melted.

In addition, it was found that the hydriding process of the machining chips contributes to eliminate steel contamination by purifying the starting material. The sintered samples showed homogeneous

microstructures, and sintering improved as particle size decreased. Casing caps in near net shape were successfully produced by means of the powder metallurgy method, indicating the feasibility of the proposed alternative to the machining method to obtain these caps.

A microstructural analysis of the samples indicated that the alloys had atypical cast Zircaloy morphology, and the rolling results confirmed that the samples met the conditions required for this process. However, further studies are needed to improve ductility.

Lastly, this study demonstrates the feasibility of recycling Zircaloy machining chips by remelting them in electric arc furnaces, which renders their properties suitable for thermomechanical processing [21,22].

Acknowledgements

The authors gratefully acknowledge the Nuclear Industries of Brazil S.A. (INB) for providing the machining chips used in this study. We are also indebted to CNPq (Brazil's National Council for Scientific and Technological Development) for awarding Project No. 483686/2010-7, and to CNEN (National Nuclear Energy Commission) for awarding a doctoral scholarship to Pereira LAT.

References

1. Mukherjee P, Chattopadhyay SK, Chatterjee SK, Meikap AK, Barat P, et al. (2000) Microstructural studies on lattice imperfections in deformed zirconium-base alloys by X-ray diffraction. Metall Mater Trans 31: 2405-2409.
2. Collins ED, Delcul GD, Spencer BB, Brunson RR, Johnson JA, et al. (2012) Process development studies for zirconium recovery/recycle from used nuclear fuel cladding. Procedia Chem 7: 72-76.
3. Bohe AE, Andrade Gamboa jj, Lopasso EM, Pasquevich DM (1996) Zirconium recovery from Zircaloy shavings. J Mater Sci 31: 3469-3474.
4. Parkison AJ, Mcdeavitt SM (2011) Hydride Formation Process for the Powder Metallurgical Recycle of Zircaloy from Used Nuclear Fuel. Metall Mater Trans A 42: 192-201.
5. Zielinski A, Sobieszczyk S (2011) Hydrogen-enhanced degradation and oxide effects in zirconium alloys for nuclear applications. Int J Hydrogen Energy 36: 8619-8629.
6. Standard specification for hot-rolled and cold-finished zirconium and zirconium alloy bars, rod, and wire for nuclear application. ASTM: B351-08. ASTM-AMERICAN Soc Test Mater.
7. Duriez C, Dupont T, Schmet B, Enoch F (2008) Zircaloy-4 and M5® high temperature oxidation and nitriding in air. J Nucl Mater 380: 30-45.
8. Pereira LAT (2014) Desenvolvimento de processos de reciclagem de cavacos de zircaloy via refusão em forno elétrico a arco e metalurgia do pó. Inst Pesqui Energéticas e Nucl - IPEN Tese.
9. Tsuchiya B, Teshigawara M, Konashi K, Yamawaki M (2002) Thermal diffusivity and electrical resistivity of zirconium hydride. J Alloys Compd 330-332: 357-360.
10. Oh SJ, Jang C, Kim JH, Jeong YH (2011) Microstructure and hydride embrittlement of zirconium model alloys containing niobium and tin. Mater Sci Eng A Elsevier B.V 528: 3771-3776.
11. Sato IM, Pereira LAT, Scapin MA, Cotrim MB, Mucsi CS, et al. (2011) Chemical and microstructural characterization of remelted Zircaloy by X-ray fluorescence techniques and metallographic analysis. J Radioanal Nucl Chem 294: 283-288.
12. Yilmazbayhan A, Motta AT, Comstock RJ, Sabol GP, Lai B, et al. (2004) Structure of zirconium alloy oxides formed in pure water studied with synchrotron radiation and optical microscopy: relation to corrosion rate. J Nucl Mater 324: 6-22.
13. Vander Voort GF (1999) Metallography - Principles and Practice. Metallography - Principles and Practice. ASM International.
14. Kim YS, Wang W, Olander DR, Yagnik SK (1996) High-pressure hydriding of Zircaloy. J Nucl Mater 240: 27-31.
15. Muntasell J, Navarro J (1985) Recovery and recrystallization of Zircaloy-4. Thermochim Acta 87: 169-176.
16. CRM 098. Certified Reference Material BCR-Commission of the European Communities. Brussels, Belgium: Commission of the European Communities.
17. Richerson DW (1992) Modern Ceramic Engineering. 2nd ed. Dekker M 846.
18. Danielson PE (2004) Metallographic techniques for zirconium and zirconium alloys. In: Metals Handbook. American Society for Metals-ASM 497-502.
19. Callister WDJ (1991) Materials Science and Engineering: an Introduction. 5th ed. New York: John Wiley & Sons, Inc 126-146-S161.
20. Olander D, Motta A (2009) Zirconium Alloys. In: Light-Water Reactor Materials 1-39.
21. Béchade JL, Menut D, Doriot S, Schlutig S, Sitaud B (2013) X-ray diffraction analysis of secondary phases in zirconium alloys before and after neutron irradiation at the MARS synchrotron radiation beamline. J Nucl Mater 437: 365-372.
22. Gamba NS, Carbajal-Ramos IA, Ula MA, Pierini BT, Gennari FC (2013) Zirconium alloys produced by recycling zircaloy tunings. J Alloys Compd. Elsevier B.V 578: 553-558.